Energy levels, absorption oscillator strengths, transition probabilities, polarizabilities, and *g* factors of Ar^{13+} ions

Lei Wu,[1] Jun Jiang,[1,*] Zhong-Wen Wu,[1] Yong-Jun Cheng,[2] Gediminas Gaigalas,[3] and Chen-Zhong Dong[1]

[1]*Key Laboratory of Atomic and Molecular Physics and Functional Materials of Gansu Province, College of Physics and Electronic Engineering, Northwest Normal University, Lanzhou 730070, People's Republic of China*

[2]*School of Physics and Information Technology, Shaanxi Normal University, Xian 710119, People's Republic of China*

[3]*Institute of Theoretical Physics and Astronomy, Vilnius University, Saulėtekio Avenue 3, 10222 Vilnius, Lithuania*

(Received 30 November 2021; revised 1 May 2022; accepted 27 June 2022; published 15 July 2022)

An accurate determination of various parameters of Ar^{13+} is presented in this work. The wave functions and energy levels of the low-lying states within the configurations of $2s^22p$ and $2s2p^2$ are calculated using the fully relativistic multiconfiguration Dirac-Hartree-Fock method, while the wave functions of higher excited states with the configurations $2s^2nl$ ($n \geqslant 3$, $l = s, p, d$) are obtained using the relativistic configuration interaction plus core polarization method. Then, the absorption oscillator strengths, transition probabilities, polarizabilities, and *g* factors are determined. The contributions of electron correlation effects, Breit interaction, and quantum electrodynamics effects are also investigated. The present results agree well with the available theoretical and experimental results. The *g* factors of the $2s^22p\ ^2P_{1/2,3/2}$ states agree with the experimental measurements on a level of 10^{-6}.

DOI: 10.1103/PhysRevA.106.012810

I. INTRODUCTION

The atomic data for highly charged ions (HCIs) are of immense interest in many areas of physics, such as diagnosing fusion and astrophysical plasma [1,2], testing quantum electrodynamics (QED) effects [3–6], the determination of the fine-structure constant α [7,8], and electron mass [9,10]. Due to their more compact size, HCIs are less sensitive to external perturbations than neutral atoms or singly charged ions. A number of theoretical studies have demonstrated that some narrow optical transitions in HCIs are good candidates for ultrahigh-precision HCI clocks with uncertainty at the level of 10^{-19} [11–20]. However, unlike neutral atoms which can be cooled to 10^{-6} K, HCIs are difficult to cool to a very low temperature. In 2015, a new breakthrough was made in terms of the resolution of this difficulty by Schmöger *et al.* [21], who achieved the sympathetic cooling of Ar^{13+} ions to a level of 10 mK using a laser-cooled Be^+ Coulomb crystal in a cryogenic Paul trap. This experiment heralded the start of a new era in the exploration of HCIs.

The ground state of Ar^{13+} is $2s^22p_{1/2}\ ^2P_{1/2}$, and $2s^22p_{3/2}\ ^2P_{3/2}$ is a long-lived metastable state with a lifetime of about 9.57 ms [22,23]. The transition wavelength between these two states, which lies in the optical range with a natural linewidth of about 17 Hz [19], has been measured to remarkable precision by the Max-Planck-Institut für Kernphysik group in Heidelberg [24–27]. The quality factor, the ratio of transition frequency to natural linewidth, of this line is about 4×10^{13} [19]. Accordingly, Ar^{13+} is a good candidate for developing a high-precision HCI optical clock, and detailed information, such as the electric-dipole ($E1$) matrix elements, polarizabilities, and *g* factors, is thus of great importance to experiments. However, there are very limited studies of these atomic parameters that can be found in the literature. For instance, as far as we know, there is only one calculation of polarizabilities [19], obtained using the relativistic coupled-cluster (RCC) method, although they are crucial parameters for evaluating blackbody shifts.

Recently, Arapoglou *et al.* measured the *g* factor of the ground state of Ar^{13+} ions in the double-Penning-trap setup with an accuracy of 10^{-11}, i.e., 0.66364845532(93) [28]. In addition, Micke *et al.* measured the *g* factor of the $(2s^22p_{3/2})\ ^2P_{3/2}$ state using quantum-logic spectroscopy with a precision of 10^{-7}, i.e., 1.3322895(13)(56)(stat)(syst) where the first set of parentheses indicates statistical uncertainty and the second set indicates systematic uncertainty [29]. The accuracy of these two experiments is eight and four orders higher, respectively, than the previous measurements using the electron-beam ion-trap technique [30]. Therefore, they provide a superb opportunity to test the accuracy of theoretical methods. As for the theoretical calculations, various theoretical methods have been used [31–38]. However, due to the different treatments of electron correlations, the accuracy of these results is different [36,38]. It should be noted that two multiconfiguration Dirac-Hartree-Fock (MCDHF) results [37,38] which were calculated using MCDHFGME [39] and GRASP2K [40] agree with the experiments [28,29] by only three significant digits. In order to explain these big differences, more detailed theoretical studies are needed.

In the present work, the wave functions and energy levels of the low-lying states of Ar^{13+} ions are calculated using the MCDHF method [41,42] and the GRASP2018 package [43]. The wave functions of higher single-electron excited states

*phyjiang@yeah.net

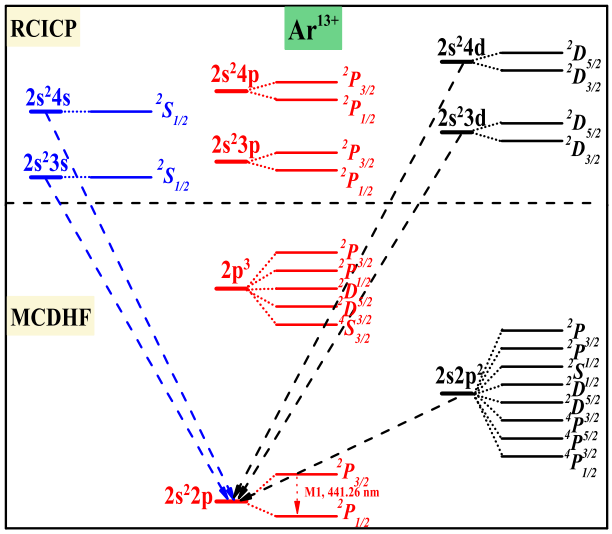

FIG. 1. Diagram of the energy-level structure of Ar^{13+} ions. It is not proportional to the energy levels.

with configurations of $2s^2nl$ $(n \geqslant 3; l = s, p, d)$ are calculated using the relativistic configuration interaction plus core polarization (RCICP) method [44]. Both methods have been verified to be capable of generating high-precision atomic parameters for many atoms and ions [42,44]. Then, the absorption oscillator strengths, transition probabilities, polarizabilities, and g factors are obtained. A detailed investigation of the contributions of electron correlation effects and Breit interaction (BI) to these atomic parameters is also presented. The present results are in good agreement with some available theoretical and experimental results.

II. THEORETICAL METHODS

In this work, the MCDHF and RCICP methods are applied in the calculation of the wave functions and energy levels of Ar^{13+} ions. The lowest excited configurations are $2s2p^2$ and $2p^3$, as illustrated in Fig. 1, formed by one or two inner-shell electron ($2s$) excitations. Thus, the electron correlation effects of these states are very strong. The wave functions of $2p^3$ were calculated in Ref. [45]. Here, we are more concerned with $2s^22p$ and $2s2p^2$. The wave functions of these states are calculated using the MCDHF method, which can accurately include the correlation effects but is more time-consuming. The higher excited states with configurations $2s^2nl$ $(n \geqslant 3; l = s, p, d)$ are calculated using the RCICP method more efficiently. Detailed descriptions of the MCDHF method were given in Refs. [41,42]; here, we just present a brief introduction.

The atomic-state wave function (ASF) is written as a linear combination of the symmetry-adapted configuration-state wave function (CSF), i.e.,

$$\Psi(\gamma PJ) = \sum_{j=1}^{N_{\mathrm{CSFs}}} c_j \Phi(\gamma_j PJ). \tag{1}$$

Here, Ψ is the ASF; Φ is the CSF, which is a linear combination of Slater determinants of one-electron Dirac orbitals; c_j is the mixing coefficient, which can be obtained by diagonalizing the Hamiltonian matrix in configuration space; J is the total angular momenta; P is parity; and γ represents other quantum numbers of corresponding states. The radial part of the Dirac orbitals is optimized by a relativistic self-consistent procedure.

In order to investigate the contribution of the electron correlation effect, the active-set approach [46] is used in the present calculations. We select $2s^22p$, $2p^3$, $2s2p3d$, and $2p3d^2$ as the reference configurations for odd-parity states and $2s2p^2$, $2p^23d$, $2s^23d$, and $2s3d^2$ for even-parity states. Then, the calculation is separated into three steps. The first step is the calculation of the core-valence (CV) correlation. In this step, the $1s$ orbital is frozen, and the active set is generated by single and double (SD) excitations to virtual orbitals from occupied orbitals in the reference configurations. The virtual orbital set is restricted to principal quantum numbers $n_{\max} = 3, 4, 5, \ldots, 11$ and orbital quantum numbers $l = 0$–4 (i.e., angular symmetries s, p, d, f, g).

The second step is the core-core (CC) correlation calculation. The $1s$ orbital is set as an active orbital as well, and the CSFs are generated by SD excitations from all occupied orbitals to virtual orbitals. Naturally, this would result in a rapid increase in the number of CSFs in the active set, as shown in Table I.

TABLE I. The number of configurations for the $J^P = 1/2^-$, $J = 3/2^-$, $J = 1/2^+$, $J = 3/2^+$, and $J = 5/2^+$ states of Ar^{13+} ions. $n_{\max}$ represents the highest principal quantum number of the virtual orbital. The superscripts $+$ and $-$ represent even and odd parity, respectively. CV and CC represent core-valence correlation and core-core correlation, respectively.

Active space	$J^P = 1/2^-$		$J^P = 3/2^-$		$J^P = 1/2^+$		$J^P = 3/2^+$		$J^P = 5/2^+$	
$n_{\max}$	CV	CC	CV	CC	CV	CC	CV	CC	CV	CC
3	52	884	78	1410	53	826	75	1289	66	1299
4	247	5919	396	10000	251	5257	394	8787	406	9834
5	675	18428	1136	32148	678	16050	1128	27809	1268	32952
6	1333	38389	2282	67704	1337	33181	2272	58203	2630	70288
7	2221	65802	3834	116668	2228	56650	3826	99969	4492	121842
8	3339	100667	5792	179040	3351	86457	5790	153107	6854	187614
9	4687	142984	8156	254802	4706	122602	8164	217617	9716	267604
10	6265	192753	10926	344008	6293	165085	10948	293499	13078	361812
11	8073	249974	14102	446604	8112	213906	14142	380753	16940	470238

TABLE II. The convergence of eigenenergy (cm^{-1}) of the ground state $2s^2 2p\ ^2P_{1/2}$ of Ar^{13+} ions.

n_{max}	CV	CC
3	−89358631	−89367916
4	−89361262	−89372671
5	−89361966	−89373696
6	−89362344	−89374354
7	−89362375	−89374942
8	−89362400	−89375229
9	−89362406	−89375458
10	−89362409	−89375488
11	−89362409	−89375496

A check of the convergence with the active set is shown in Table II, where the eigenenergies of the ground state $2s^2 2p\ ^2P_{1/2}$ generated in expanding the active set are listed. It is reasonable for the CV calculation to achieve convergence rapidly, while it is relatively slow for the CC calculation. As a further check, we also calculated the triple excitation based on the $n_{max} = 11$ CC calculation, which is not shown for simplicity. The contribution is found to be only 3 cm^{-1} for the ground state. We also list the energy levels of the excited states relative to the ground state in Table III. We can find that the contributions of the CC correlation are approximately from 10^2 to 10^3 cm^{-1}. All calculations are well converged when n_{max} is increased to 11. The extrapolated values are obtained from exponential extrapolation using the results of $n_{max} = 8, 9, 10$, and 11 CC calculations. The third step is the calculation of the Breit interaction, QED effects, and nuclear recoil corrections. In this step, we reperformed the configuration interaction calculation, in which these effects are added to the Hamiltonian [42] and the Hamiltonian matrix is rediagonalized. The N-electron Breit interaction can be written as [47]

$$H_{\rm Breit} = -\sum_{i<j}^{N}\left[\boldsymbol{\alpha}_i\cdot\boldsymbol{\alpha}_j\frac{\cos(\omega_{ij}r_{ij}/c)}{r_{ij}} + (\boldsymbol{\alpha}_i\cdot\Delta_i)(\boldsymbol{\alpha}_j\cdot\Delta_j)\frac{\cos(\omega_{ij}r_{ij}/c)-1}{\omega_{ij}^2 r_{ij}/c^2}\right], \quad (2)$$

where $r_{ij} = |\boldsymbol{r}_i - \boldsymbol{r}_j|$ is the distance between two electrons. ω_{ij} is the photon energy exchanged between two electrons. $\boldsymbol{\alpha}_i$ is the Dirac matrix, and c is the speed of light. Since the Breit interaction is included in the Hamiltonian, its contribution is reflected in the variation of mixing coefficients and energy levels.

The QED corrections are separated into two classes, namely, self-energy (SE) and vacuum polarization (VP). The total SE contribution is given as the sum of one-electron corrections weighted by the fractional occupation number of the one-electron orbital in the total wave functions [48–50], i.e.,

$$H^{\rm SE} = \sum_i q_i E_i^{\rm SE}. \quad (3)$$

TABLE III. The convergence of the energy levels (cm^{-1}) of some low-lying excited states of Ar^{13+} ions. The extrapolated values are exponential extrapolations using the results of $n_{max} = 8, 9, 10$, and 11 core-core correlation calculations. The numbers in the parentheses represent uncertainties.

Active space	$2s^2 2p$	$2s2p^2$							
n_{max}	$^2P_{3/2}$	$^4P_{1/2}$	$^4P_{3/2}$	$^4P_{5/2}$	$^2D_{3/2}$	$^2D_{5/2}$	$^2S_{1/2}$	$^2P_{1/2}$	$^2P_{3/2}$
					CV				
3	23682	229166	238123	250846	415264	416536	521081	552457	562613
4	23688	229795	238562	251276	414619	415913	519677	551160	561368
5	23692	229971	238948	251656	412737	414037	516401	548679	559157
6	23693	230153	239132	251839	412557	413860	516018	548383	558890
7	23693	230187	239167	251874	412487	413790	515879	548275	558791
8	23694	230213	239193	251902	412402	413784	515869	548264	558779
9	23692	230225	239206	251917	412399	413780	515864	548246	558767
10	23692	230229	239210	251922	412392	413778	515863	548242	558762
11	23692	230230	239211	251924	412390	413777	515863	548240	558760
					CC				
3	23784	227398	234779	246514	413702	414978	516827	549910	561146
4	23752	228999	235688	248418	413524	414123	515515	548992	559738
5	23747	229356	236950	249677	413133	413882	515345	548132	558813
6	23744	229788	237138	251292	412636	413455	515293	547502	558083
7	23742	230402	238418	251951	412396	413194	515199	546968	557298
8	23740	230430	239228	252121	411944	413122	515152	546595	556792
9	23740	230443	239655	252153	411864	413097	515114	546496	556566
10	23740	230458	239659	252186	411842	413059	515057	546463	556493
11	23740	230461	239662	252190	411834	413047	515041	546441	556466
Extrapolated	23741(1)	230476(15)	239671(9)	252212(22)	411831(3)	412957(90)	514929(112)	546432(9)	556454(12)

TABLE IV. The first three dominant mixing coefficients for the $2s^2 2p\ ^2P_{1/2}$ and $^2P_{3/2}$ states. "CI+Breit+SE+VP+Nuclear recoil" indicates the Breit interaction, self-energy, vacuum polarization, and nuclear recoil corrections are included in the configuration interaction calculations.

		$2s^2 2p\ ^2P_{1/2}$		
Configuration	$(1s^2 2s^2)_0 2p_{1/2}$	$(1s^2 2p_{3/2}^2)_0 2p_{1/2}$	$[(1s^2 2s_{1/2}\, 2p_{1/2})_1 3d_{3/2}]_{1/2}$	Eigenenergy (cm^{-1})
CI	0.985227	0.166976	−0.022176	−89375496
CI+Breit	0.985340	0.166703	−0.021843	−89355118
CI+Breit+SE	0.985279	0.166817	−0.021850	−89334392
CI+Breit+SE+VP	0.985282	0.166795	−0.021847	−89335856
CI+Breit+SE+VP+Nuclear recoil	0.985279	0.166801	−0.021849	−89334668
		$2s^2 2p\ ^2P_{3/2}$		
Configuration	$(1s^2 2s^2)_0 2p_{3/2}$	$(1s^2 2p_{1/2}^2)_0 2p_{3/2}$	$(1s^2)_0 2p_{3/2}^3$	Eigenenergy (cm^{-1})
CI	0.984354	0.124963	0.117541	−89351756
CI+Breit	0.984474	0.124272	0.117401	−89332507
CI+Breit+SE	0.984405	0.124563	0.117632	−89311733
CI+Breit+SE+VP	0.984409	0.124544	0.117612	−89313198
CI+Breit+SE+VP+Nuclear recoil	0.984406	0.124563	0.117622	−89312011

Here, q_i is the occupation number of orbital i. $E_i^{\rm SE}$ is expressed as [48–50]

$$E_i^{\rm SE} = \frac{Z^4}{\pi c^3 n_i^3} F_i(Z/c), \tag{4}$$

where n_i is the principal quantum number, Z is the nuclear charge, and $F_i(Z/c)$ is a slowly varying function of Z/c that was tabulated by Mohr [51] and Klarsfeld and Maquet [52]. In our calculation, this SE correction is included in the diagonal elements of the Hamiltonian matrix. Therefore, the changes in mixing coefficients and eigenvalues represent the SE contribution.

To the lowest order, the VP correction is a short-range modification of the nuclear field due to screening by virtual electron-positron pairs [53,54]. It is written as [54]

$$H^{\rm VP} = \sum_i q_i \int_0^\infty V^{\rm VP}(r)[P_i^2(r) + Q_i^2(r)]dr, \tag{5}$$

where $P_i(r)$ and $Q_i(r)$ are the large and small components of radial wave functions, respectively. $V^{\rm VP}$ is the VP potential [53].

In the present calculation, the nuclear recoil is expressed in the lowest-order nuclear motional corrections [42], namely, normal mass shift (NMS),

$$H_{\rm NMS} = \frac{1}{M}\sum_{i=1}^{N}[c\boldsymbol{\alpha}_i \cdot \boldsymbol{p}_i + c^2(\beta_i - 1)], \tag{6}$$

and specific mass shift (SMS),

$$H_{\rm SMS} = \frac{1}{M}\sum_{j>i=1}^{N} \boldsymbol{p}_i \boldsymbol{p}_j, \tag{7}$$

where M is the nuclear mass in atomic units and $\boldsymbol{p}_i$ is the electron momentum operator.

Since the energy levels of the single-electron excited states $2s^2 nl$ $(n \geqslant 3; l = s, p, d)$ are much higher than those of $2s2p^2$, the wave functions and energy levels of $2s^2 nl$ $(n \geqslant 3; l = s, p, d)$ states are calculated by using a relativistic semiempirical method: the RCICP method [44]. The basic strategy of RCICP is to partition the electrons into a $1s^2 2s^2$ core plus a valence electron. The core orbitals are calculated using the Dirac-Fock method, and the core-valence correlation is calculated by adding an effective polarization potential to the Hamiltonian. The polarization potential $V_{\rm p}(\boldsymbol{r})$ is treated semiempirically as follows:

$$V_{\rm p}(\boldsymbol{r}) = -\sum_{k=1}^{2} \frac{\alpha_{\rm core}^{(k)}}{2r^{2(k+1)}} \sum_{\ell,J} g_{\ell,J}^2(r)|\ell J\rangle\langle \ell J|. \tag{8}$$

$\alpha_{\rm core}^{(k)}$ is the kth-order static polarizabilities of the core electrons, where $\alpha_{\rm core}^{(1)} = 9.0(1)\times 10^{-5}$ a.u. and $\alpha_{\rm core}^{(2)} = 1.0\times 10^{-6}$ a.u. are calculated using the two-valence-electron RCICP method. $g_{\ell,J}^2(r) = 1 - \exp(-r^{2(k+2)}/\rho_{\ell,J}^{2(k+2)})$, and the cutoff parameters $\rho_{\ell,J}$ are tuned to reproduce the binding energies of the ground state and some single-electron excited states. The adopted parameters are $\rho_{s_{1/2}} = 1.313$, $\rho_{p_{1/2}} = 0.905$, $\rho_{p_{3/2}} = 0.898$, $\rho_{d_{3/2}} = 0.798$, and $\rho_{d_{5/2}} = 0.788$ a.u. The effective Hamiltonian of the valence electron is diagonalized within a large S-spinor and L-spinor basis [55,56] which can be regarded as a relativistic generalization of the Slater-type and Laguerre-type orbitals.

III. RESULTS AND DISCUSSION

A. Energy levels

As we have stated, the wave functions and energy levels of Ar^{13+} ions are calculated using the method described above. Table IV lists the first three dominant mixing coefficients for the $2s^2 2p\ ^2P_{1/2}$ and $^2P_{3/2}$ states. The dominant configurations are $(1s^2 2s^2)_0 2p_{1/2}$ and $(1s^2 2p_{3/2}^2)_0 2p_{1/2}$ for the ground state $^2P_{1/2}$, while the dominant configurations are $(1s^2 2s^2)_0 2p_{3/2}$, $(1s^2 2p_{1/2}^2)_0 2p_{3/2}$, and $(1s^2)_0 2p_{3/2}^3$ for the $^2P_{3/2}$ state. Table V lists the generated energy levels of the low-lying states and the contributions of the Breit interaction, QED effects, and nuclear recoil correction, along with a comparison with some available theoretical results [24,45,57–60] as well as the National Institute of Science and Technology (NIST) tabulations [61]. For the $2s^2 2p\ ^2P_{3/2}$ state, the contribution of

TABLE V. Comparison of the energy levels (cm^{-1}) and the contributions of Breit interaction, SE, VP and nuclear recoil for the low-lying excited states of Ar^{13+} ions with some available theoretical results [24,45,57–60] and experimental results of the NIST tabulation [61]. The energy levels are given relative to the ground state.

	$2s^22p\ ^2P_{3/2}$		$2s2p^2\ ^4P_{1/2}$		$2s2p^2\ ^4P_{3/2}$	
Model	This work	Other studies	This work	Ref. [57]	This work	Ref. [57]
CI	23741(1)	23737 [45] 23921 [57]	230476(15)	224126	239671(9)	233070
Breit	−1129(7)	−1131 [45] −1136 [57]	628(193)	479	−85(35)	45
VP	−1(1)	−3 [45]	64(43)		64(43)	
SE	48(3)	51 [45]	−945(59)		−923(58)	
QED (VP+SE)	47(3)	47 [45] 49.5(70) [24] 10 [57] 51.2(2.0) [58] 44 [59]	−881(73)	−1301	−859(72)	−1292
Nuclear recoil	−1(1)	−0.6 [58]	−56(37)		−114(76)	
Total	22658(8)	22653 [45] 22795 [57] 22662(14) [24] 22656.1(3.6) [58] 22659 [59] 22657 [60]	230167(210)	223304	238613(111)	231823
NIST [61]	22656		230296		238954	
	$2s2p^2\ ^4P_{5/2}$		$2s2p^2\ ^2D_{3/2}$		$2s2p^2\ ^2D_{5/2}$	
Model	This work	Ref. [57]	This work	Ref. [57]	This work	Ref. [57]
CI	252212(22)	245812	411831(3)	418209	412957(90)	419451
Breit	−1122(291)	−1235	−439(114)	−489	−793(206)	−844
VP	64(43)		69(46)		66(44)	
SE	−897(56)		−917(57)		−908(57)	
QED (VP+SE)	−833(70)	−1280	−848(73)	−1375	−842(72)	−1371
Nuclear recoil	−56(37)		−58(39)		−59(39)	
Total	250201(302)	243297	410486(141)	416345	411263(239)	417236
NIST [61]	250423		410254		411205	
	$2s2p^2\ ^2S_{1/2}$		$2s2p^2\ ^2P_{1/2}$		$2s2p^2\ ^2P_{3/2}$	
Model	This work	Ref. [57]	This work	Ref. [57]	This work	Ref. [57]
CI	514929(112)	521271	546432(9)	557941	556454(12)	569207
Breit	546(142)	581	−146(67)	−76	−864(224)	−889
VP	66(44)		68(45)		69(46)	
SE	−934(58)		−908(57)		−899(56)	
QED (VP+SE)	−868(73)	−1401	−840(73)	−1525	−830(73)	−1546
Nuclear recoil	−57(38)		−60(40)		−50(33)	
Total	514550(199)	520451	545386(107)	556340	554710(238)	566772
NIST [61]	514401		545244		554678	

the Breit interaction is significant, and the present result is in good agreement with the calculations from Refs. [45,57]; the difference is less than 0.6%. In Refs. [58,59], the values of the one-electron Dirac energy and electron-correlation effects within the Breit approximation are given in detail. The summations of these values are 22605.5(3.0) cm^{-1} [58] (the average value of the four different potential calculations) and 22616 cm^{-1} [59]. The sum of our configuration interaction (CI) value and the contribution of the Breit interaction, 22612 cm^{-1}, is in excellent agreement with these results. The differences are less than 0.03%. The present calculations of QED effects also agree very well with the rigorous bound-state QED results for the first-order [24] and second-order [58,59] diagrams. In Table V, the result of Ref. [58] is 51.2(2.0) cm^{-1}, which is the average value of four different types of the screening-potential calculations, including first, second, third, and higher order, as well as two-loop QED. The contribution of nuclear recoil is very small and is about −1 cm^{-1}, which indicates that the contribution of nuclear recoil to $^2P_{3/2}$ is almost the same as that to the ground state. The present result agrees well with the calculation in Ref. [58]. The present energy level labeled "Total" shows excellent

TABLE VI. Comparison of energy levels (cm^{-1}) of the single-electron excited states $2s^2nl$ ($n = 3, 4$; $l = s, p, d$) of Ar^{13+} ions with theoretical results of the many-body perturbation theory (MBPT) [62] and the MCDHF method [63] and experimental results of the NIST tabulation [61]. The energy levels are given relative to the ground state.

States	RCICP	MBPT [62]	MCDHF [63]	NIST [61]
$2s^23s\ ^2S_{1/2}$	3417243	3417865	3410207	
$2s^23p\ ^2P_{1/2}$	3533681	3530600	3524071	3533890
$2s^23p\ ^2P_{3/2}$	3534598	3536817	3530293	3534840
$2s^23d\ ^2D_{3/2}$	3640469	3641742	3636442	3640470
$2s^23d\ ^2D_{5/2}$	3641775	3643496	3638165	3641780
$2s^24s\ ^2S_{1/2}$	4629027		4628983	
$2s^24p\ ^2P_{1/2}$	4681863		4675083	
$2s^24p\ ^2P_{3/2}$	4684168		4677640	
$2s^24d\ ^2D_{5/2}$	4724201		4715620	4722050
$2s^24d\ ^2D_{3/2}$	4727900		4716323	4724300

agreement with the NIST result [61] and the calculations from Refs. [24,45,58–60], with a difference of no more than 0.02%.

As for the states of $2s2p^2$, the presently calculated contributions of the Breit interaction agree well with the results of Ref. [57]. In contrast, our results for the QED effects, which are dominated by SE, are smaller than those of Ref. [57] by about 35%. The contribution of nuclear recoil to the states of $2s2p^2$ is about 50–60 cm^{-1}, except for the $^4P_{3/2}$ state, which is about -114 cm^{-1}. The present total energy levels agree very well with the NIST tabulation [61], and the differences are less than 0.1%.

The energy levels of the single-electron excited states $2s^2nl$ ($n \geqslant 3; l = s, p, d$) are listed in Table VI and are compared with the NIST tabulation [61] and theoretical results of the many-body perturbation theory [62] and the MCDHF method [63]. The present RCICP results show good agreement with the measurements [61], and the difference is no more than 0.3%. Excellent agreement of the present energy levels with existing theoretical and experimental results indicates a high accuracy level of the wave functions.

B. Absorption oscillator strength and transition probability

The transition probability $A_{n\to i}$ (in s^{-1}) and the absorption oscillator strength $f_{i\to n}$ for the electric dipole ($E1$) transition $n \to i$ are related by the following expression [63]:

$$A_{n\to i} = \frac{8e^2\pi^2 g_i f_{i\to n}}{mc\lambda_{n\to i}^2 g_n}, \tag{9}$$

where, m and e are the electron mass and charge, respectively. $\lambda_{n\to i}$ (in Å) is the transition wavelength, and g_i and g_n are the statistical weights of the lower i and upper n states. The $E1$ absorption oscillator strength $f_{i\to n}$ is written as [64]

$$f_{i\to n} = \frac{2|\langle\Psi(\gamma_n P_n J_n)\|\boldsymbol{O}\|\Psi(\gamma_i P_i J_i)\rangle|^2 \Delta E_{n\to i}}{3(2J_i+1)}, \tag{10}$$

where $\boldsymbol{O}$ is the $E1$ transition operator and $\Delta E_{n\to i} = E_n - E_i$ is the transition energy.

Table VII lists the presently calculated absorption oscillator strengths f in Babushkin gauge (length form) and transition probabilities between the fine-structure levels of the $2s^22p$ and $2s2p^2$ configuration as well as the theoretical results of Rynkun *et al.* [65]. The subscript CC represents the results of the $n_{max} = 11$ core-core correlation calculation, and BI and QED represent the Breit interaction and QED effects. It can be seen from Table VII that the contributions of Breit interactions are about 10% to the $2s2p^2\ ^4P_{1/2}$, $^4P_{3/2} \to 2s^22p\ ^2P_{1/2}$ and $2s2p^2\ ^4P_{3/2}$, $^2S_{1/2} \to 2s^22p\ ^2P_{3/2}$ transitions. The contribution of QED effects to most transitions is less than 1%, except for the $2s2p^2\ ^4P_{3/2} \to 2s^22p\ ^2P_{3/2}$ transition, for which the contribution is close to 2%.

The present results agree well with the results of Ref. [65]. Since the QED effects are included in the Hamiltonian, the contributions are reflected in the change in mixing coefficients and energy levels. We find that the contribution of QED effects to the transition probabilities and absorption oscillator

TABLE VII. Absorption oscillator strengths f in Babushkin gauge (length form) and transition probabilities A (s^{-1}) between the fine-structure levels of $2s^22p$ and $2s2p^2$ of Ar^{13+} ions. The subscript CC represents the results of the $n_{max} = 11$ core-core correlation calculation, and BI and QED indicate the Breit interaction and QED effects are considered. The notation $a[b]$ represents $a\times10^b$. The uncertainties are given in parentheses.

Transition	f_{CC}	A_{CC}	A_{BI}	A_{BI+QED}	Ref. [65]
$2s2p^2\ ^4P_{1/2} \to 2s^22p\ ^2P_{1/2}$	9.173[−5]	3.261[6]	2.979[6]	2.957(34)[6]	2.922[6]
$2s2p^2\ ^4P_{3/2} \to 2s^22p\ ^2P_{1/2}$	4.028[−6]	7.710[4]	7.018[4]	7.056(82)[4]	7.025[4]
$2s2p^2\ ^2D_{3/2} \to 2s^22p\ ^2P_{1/2}$	6.167[−2]	3.487[9]	3.460[9]	3.437(85)[9]	3.384[9]
$2s2p^2\ ^2S_{1/2} \to 2s^22p\ ^2P_{1/2}$	8.753[−2]	1.556[10]	1.534[10]	1.529(18)[10]	1.503[10]
$2s2p^2\ ^2P_{1/2} \to 2s^22p\ ^2P_{1/2}$	3.661[−2]	7.309[9]	7.609[9]	7.548(87)[9]	7.539[9]
$2s2p^2\ ^2P_{3/2} \to 2s^22p\ ^2P_{1/2}$	3.849[−2]	3.974[9]	3.977[9]	3.955(46)[9]	3.903[9]
$2s2p^2\ ^4P_{1/2} \to 2s^22p\ ^2P_{3/2}$	2.940[−5]	1.699[6]	1.607[6]	1.594(18)[6]	1.579[6]
$2s2p^2\ ^4P_{3/2} \to 2s^22p\ ^2P_{3/2}$	1.837[−5]	5.762[5]	5.195[5]	5.133(98)[5]	5.276[5]
$2s2p^2\ ^4P_{5/2} \to 2s^22p\ ^2P_{3/2}$	1.090[−4]	2.524[6]	2.381[6]	2.360(27)[6]	2.385[6]
$2s2p^2\ ^2D_{3/2} \to 2s^22p\ ^2P_{3/2}$	2.684[−3]	2.709[8]	2.782[8]	2.757(32)[8]	2.745[8]
$2s2p^2\ ^2D_{5/2} \to 2s^22p\ ^2P_{3/2}$	4.799[−2]	3.244[9]	3.251[9]	3.227(80)[9]	3.050[9]
$2s2p^2\ ^2S_{1/2} \to 2s^22p\ ^2P_{3/2}$	5.958[−3]	1.935[9]	2.096[9]	2.081(24)[9]	2.037[9]
$2s2p^2\ ^2P_{1/2} \to 2s^22p\ ^2P_{3/2}$	4.174[−2]	1.531[10]	1.522[10]	1.515(18)[10]	1.510[10]
$2s2p^2\ ^2P_{3/2} \to 2s^22p\ ^2P_{3/2}$	1.187[−1]	2.256[10]	2.259[10]	2.247(56)[10]	2.131[10]

TABLE VIII. Absorption oscillator strengths between the fine-structure levels of $2s^22p$ and $2s^2nl$ ($n = 3, 4; l = s, d$) of Ar^{13+} ions. SST represents the results calculated using SUPERSTRUCTURE [66].The notation $a[b]$ indicates $a\times10^b$. The uncertainties are given in parentheses.

Transition	RCICP	SST [66]
$2s^22p\ ^2P_{1/2} \rightarrow 2s^23s\ ^2S_{1/2}$	2.302(750)[−2]	3.013[−2]
$2s^22p\ ^2P_{1/2} \rightarrow 2s^23d\ ^2D_{3/2}$	6.091(188)[−1]	6.235[−1]
$2s^22p\ ^2P_{1/2} \rightarrow 2s^24s\ ^2S_{1/2}$	4.781(148)[−3]	
$2s^22p\ ^2P_{1/2} \rightarrow 2s^24d\ ^2D_{3/2}$	1.239(38)[−1]	
$2s^22p\ ^2P_{3/2} \rightarrow 2s^23s\ ^2S_{1/2}$	2.389(777)[−2]	1.712[−2]
$2s^22p\ ^2P_{3/2} \rightarrow 2s^23d\ ^2D_{3/2}$	6.137(189)[−2]	6.358[−2]
$2s^22p\ ^2P_{3/2} \rightarrow 2s^23d\ ^2D_{5/2}$	5.529(171)[−1]	5.720[−1]
$2s^22p\ ^2P_{3/2} \rightarrow 2s^24s\ ^2S_{1/2}$	4.931(152)[−3]	
$2s^22p\ ^2P_{3/2} \rightarrow 2s^24d\ ^2D_{3/2}$	1.237(38)[−2]	
$2s^22p\ ^2P_{3/2} \rightarrow 2s^24d\ ^2D_{5/2}$	1.117(34)[−1]	

strengths is mainly caused by the change in transition energy. However, the change in mixing coefficients has little effect on the transition probabilities. In addition, the contributions of nuclear recoil to the transition probabilities are one or two orders of magnitude smaller than that of the QED effects. Therefore, the contribution of nuclear recoil is not given in Table VII.

Table VIII lists some of the absorption oscillator strengths between the fine-structure levels of $2s^22p$ and $2s^2nl$ ($n = 3, 4; l = s, d$) calculated using the RCICP method. The present results agree well with the calculation using the SUPERSTRUCTURE (SST) code [66].

C. The static $E1$ polarizabilities

If an atom is placed in an electrostatic field, the lowest-order energy shift due to the Stark effect can be written as

$$\Delta E_{\rm Stark} \approx -\tfrac{1}{2}\alpha F^2, \tag{11}$$

where F is the strength of the electrostatic field. α is static $E1$ polarizability. The $E1$ polarizability for a state with angular momentum $J_i = 1/2$ is independent of the magnetic projection M_i, while for $J_i > 1/2$ it depends on M_i, i.e., via scalar (α^S) and tensor (α^T) components:

$$\alpha = \alpha^S + \frac{3M_i^2 - J_i(J_i+1)}{J_i(2J_i-1)}\alpha^T. \tag{12}$$

The scalar and tensor polarizabilities are usually defined in terms of a sum over all possible intermediate states, excluding the initial state while including the continuum,

$$\alpha^S = \sum_n \frac{f_{i\rightarrow n}}{\Delta E_{n\rightarrow i}^2} \tag{13}$$

and

$$\alpha^T = 6\sqrt{\frac{5J_i(2J_i-1)(2J_i+1)}{6(J_i+1)(2J_i+3)}} \times \sum_n (-1)^{J_n+J_i} \begin{Bmatrix} 1 & 1 & 2 \\ J_i & J_i & J_n \end{Bmatrix} \frac{f_{i\rightarrow n}}{\Delta E_{n\rightarrow i}^2}. \tag{14}$$

TABLE IX. Static $E1$ scalar α^S and tensor α^T polarizabilities (in a.u.) of the $2s^22p\ ^2P_{1/2,3/2}$ states and the breakdown of the contributions of individual transitions for Ar^{13+} ions. "Remains" represents the contributions from highly excited bound and continuum states of the valence electrons. "Core" denotes the contributions of the core ($1s^2$) electrons. The uncertainties are given in parentheses.

	$2s^22p\ ^2P_{1/2}$	$2s^22p\ ^2P_{3/2}$	
Up levels	α^S	α^S	α^T
$2s2p^2\ ^4P_{1/2}$	0.00008(1)	0.00003(0)	−0.00003(0)
$2s2p^2\ ^4P_{3/2}$	0.00000(0)	0.00002(0)	0.00001(0)
$2s2p^2\ ^4P_{5/2}$		0.00009(1)	−0.00002(1)
$2s2p^2\ ^2D_{3/2}$	0.01738(43)	0.00087(1)	0.00070(1)
$2s2p^2\ ^2D_{5/2}$		0.01522(38)	−0.00304(38)
$2s2p^2\ ^2S_{1/2}$	0.01564(18)	0.00127(2)	−0.00127(2)
$2s2p^2\ ^2P_{1/2}$	0.00612(7)	0.00728(9)	−0.00728(9)
$2s2p^2\ ^2P_{3/2}$	0.00600(7)	0.02012(50)	0.01610(50)
$2s^23s\ ^2S_{1/2}$	0.00009(3)	0.00010(3)	−0.00010(3)
$2s^23d\ ^2D_{3/2}$	0.00221(7)	0.00023(2)	0.00018(2)
$2s^23d\ ^2D_{5/2}$		0.00203(7)	−0.00041(7)
$2s^24s\ ^2S_{1/2}$	0.00001(1)	0.00001(0)	−0.00001(0)
$2s^24d\ ^2D_{3/2}$	0.00027(3)	0.00003(0)	0.00002(0)
$2s^24d\ ^2D_{5/2}$		0.00024(2)	−0.00005(2)
Remains	0.00038(3)	0.00042(3)	0.00011(1)
Core ($1s^2$)	0.00009(1)	0.00009(1)	
Total	0.04827(48)	0.04807(64)	0.00491(64)
Ref. [19]	0.0484(1)	0.0482(1)	

As illustrated in Fig. 1, the main contributions to the polarizabilities of the $2s^22p\ ^2P_{1/2,\,3/2}$ states are the transitions of the $2s2p^2$ and $2s^2nl$ ($n = 3, 4; l = s, d$) states. Table IX lists the static $E1$ polarizabilities of the $2s^22p\ ^2P_{1/2,\,3/2}$ states and the breakdown of the contributions of individual transitions. We can find that the polarizability of the $^2P_{1/2}$ state is dominated by $2s2p^2\ ^2D_{3/2} \rightarrow 2s^22p\ ^2P_{1/2}$ and $2s2p^2\ ^2S_{1/2} \rightarrow 2s^22p\ ^2P_{1/2}$ transitions, while for the $^2P_{3/2}$ state it is dominated by the $2s2p^2\ ^2D_{5/2} \rightarrow 2s^22p\ ^2P_{3/2}$ and $2s2p^2\ ^2P_{3/2} \rightarrow 2s^22p\ ^2P_{3/2}$ transitions. "Remains" in Table IX represents the contributions from highly excited bound and continuum states of the valence electrons, which are calculated using the RCICP method. "Core" denotes the contributions of the core ($1s^2$) electrons, which are determined by the calculation of the polarizability of He-like Ar^{16+} ions. We can see that the present total scalar polarizabilities α^S are in good agreement with the results of the RCC method [19]. The difference is no more than 0.5%. The tensor polarizability α^T of the $2s^22p\ ^2P_{3/2}$ state is 0.00491(64) a.u., which is one order smaller than α^S. There are no other results for α^T available for comparison.

D. Landé g factor

The first-order Zeeman energy shift of an atomic state, which is dependent on the magnetic projections M, can be written as

$$\Delta E_{\rm Zeeman} = g\mu_B BM, \tag{15}$$

where B is the strength of the magnetic field and μ_B is the Bohr magneton. g is the Landé g factor of the electronic state.

TABLE X. The convergence of the g factor for the $2s^2 2p\ ^2P_{1/2,3/2}$ states of Ar^{13+} ions, which are calculated under the core-core correlation model. $\Delta g_{\rm PS} = g - g_D$ represents only the contribution of positive-energy states.

Active space $n_{\max}$	$2s^2 2p\ ^2P_{1/2}$		$2s^2 2p\ ^2P_{3/2}$	
	g	$\Delta g_{\rm PS} = g - g_D$	g	$\Delta g_{\rm PS} = g - g_D$
Single configuration	0.664505776	0.000730329	1.331575281	0.000544892
3	0.664501682	0.000726235	1.331574903	0.000544514
4	0.664496449	0.000721002	1.331574163	0.000543774
5	0.664494773	0.000719326	1.331573776	0.000543387
6	0.664493971	0.000718524	1.331573674	0.000543285
7	0.664493622	0.000718175	1.331573611	0.000543222
8	0.664493416	0.000717969	1.331573585	0.000543196
9	0.664493371	0.000717924	1.331573576	0.000543187
10	0.664493323	0.000717876	1.331573573	0.000543184
11	0.664493322	0.000717875	1.331573572	0.000543183

If the electron-electron interactions are neglected, the leading contribution to the g factor can be evaluated analytically by using analytic Dirac wave functions corresponding to a pointlike nucleus, namely [67],

$$g_D = \frac{\kappa}{2J(J+1)}(2\kappa\varepsilon_{n\kappa} - 1), \tag{16}$$

where κ is the relativistic quantum number and $\varepsilon_{n\kappa}$ is the Dirac energy of the reference state. For the $2s^2 2p\ ^2P_{1/2}$ and $2s^2 2p\ ^2P_{3/2}$ states of Ar^{13+} ions, g_D are 0.663775447 and 1.331030389, respectively.

Using the projection theorem [68], the Landé g factor can be expressed as [69]

$$g = \frac{1}{2\mu_B}\frac{\langle\Psi(\gamma PJ)\rangle||\boldsymbol{N}^{(1)}||\Psi(\gamma PJ)\rangle}{\sqrt{J(J+1)(2J+1)}}, \tag{17}$$

where $\boldsymbol{N}^{(1)} = \sum_{q=0,\pm1}\boldsymbol{N}_q^{(1)}$ and $\boldsymbol{N}_q^{(1)} = -\sum_j i\sqrt{\frac{8\pi}{3}}r_j\boldsymbol{\alpha}_j \cdot \boldsymbol{Y}_{1q}^{(0)}(\hat{\boldsymbol{r}}_j)$ is an operator of the same tensorial form as the magnetic dipole hyperfine operator [69]. $i = \sqrt{-1}$ is the imaginary unit, r_j is the coordinate of electron j, $\boldsymbol{\alpha}_j$ denotes the Dirac matrices, and $\boldsymbol{Y}_{1q}^{(0)}$ represents the vector spherical harmonic [70].

Table X lists the presently calculated CC-model g values of $^2P_{1/2}$ and $^2P_{3/2}$ states, in which only positive-energy states are included. It shows a very good convergence. Table X also lists the difference ($\Delta g_{\rm PS}$) between the calculated g and the analytic Dirac value g_D. These $\Delta g_{\rm PS}$ values represent the contribution of the electron correlations of positive-energy states, and they converge to 0.00071787(1) and 0.00054318(1) for the $^2P_{1/2}$ and $^2P_{3/2}$ states, respectively.

Besides the positive-energy states, the negative-energy states (NSs) and Breit interaction also play an important role. Here, the contribution of negative-energy states is also calculated. In our calculation, the negative-energy orbitals are generated based on the RCICP method. Then, we performed the CI calculations, in which the positive-energy orbitals of $n \geqslant 6$ are replaced by the negative-energy orbitals and the orbitals of $n \leqslant 5$ remain unchanged. In addition, the Breit interaction is also included. Table XI lists the presently calculated g factors. Since the $n \geqslant 6$ orbitals are replaced with the negative-energy orbitals, the difference between these results and 5 CC results represents the contribution of the negative-energy states ($\Delta g_{\rm NS} = g - g_{\rm 5CC}$). It can be seen that the contribution of NSs converges to -0.00006669 with the increase of the negative-energy orbitals, but the convergence speed is very slow.

TABLE XI. The g factor of the $2s^2 2p\ ^2P_{1/2,3/2}$ states and the contributions of negative-energy states. In the calculations, the Breit interaction is included, and the orbitals with $n \geqslant 6$ are replaced by the negative-energy orbitals. NCSF represents the number of configurations of negative-energy states. $\Delta g_{\rm NS}$ represents the contribution of the negative-energy states and Breit interaction to g factors.

Active space $n_{\max}$	$2s^2 2p\ ^2P_{1/2}$			$2s^2 2p\ ^2P_{3/2}$		
	NCSF	g	$\Delta g_{\rm NS} = g - g_{\rm 5CC}$	NCSF	g	$\Delta g_{\rm NS} = g - g_{\rm 5CC}$
6	3468	0.664435383	−0.000059390	6029	1.331518352	−0.000055424
7	8118	0.664433766	−0.000061007	14142	1.331517415	−0.000056361
8	13950	0.664432283	−0.000062490	24339	1.331516492	−0.000057284
9	20965	0.664431062	−0.000063711	36621	1.331515589	−0.000058187
10	29161	0.664430058	−0.000064715	50986	1.331514789	−0.000058987
11	38539	0.664429247	−0.000065526	67435	1.331513989	−0.000059787
12	43492	0.664428451	−0.000066322	76067	1.331513336	−0.000060440
13	49000	0.664427944	−0.000066829	85670	1.331513027	−0.000060749
14	55062	0.664427837	−0.000066936	96243	1.331513015	−0.000060761
15	61678	0.664427834	−0.000066939	107786	1.331513011	−0.000060765

TABLE XII. The contributions of SE, VP, and nuclear recoil, which are included in the Hamiltonian, to g factors for the $2s^2 2p\ ^2P_{1/2,3/2}$ states of Ar^{13+} ions.

Contribution	$2s^2 2p\ ^2P_{1/2}$	$2s^2 2p\ ^2P_{3/2}$
$\Delta g_{\rm SE}$	4.0×10^{-9}	4.4×10^{-8}
$\Delta g_{\rm VP}$	3.0×10^{-9}	1.0×10^{-9}
$\Delta g_{\rm Nuclear\ recoil}$	2.2×10^{-8}	1.3×10^{-8}

The contributions of QED effects to the g factors are very important as well. In our calculations, they can be divided into two parts. In the first part, as we have discussed above, the QED effects are included in the Hamiltonian. In this case, they affect the wave functions and then the g factor. However, we found that these effects are only at a level of 10^{-8}, as shown in Table XII. The second part is the corrections to the magnetic-field interaction operator, which can be written as (see Refs. [69,70] for details)

$$\Delta g_{\rm QED}=\frac{(g_s-2)\langle\Psi(\gamma PJ)\rangle||\Delta \boldsymbol{N}^{(1)}||\Psi(\gamma PJ)\rangle}{2\sqrt{J(J+1)(2J+1)}}, \tag{18}$$

where g_s= 2.0023193 [71] is the correction value of the free-electron g factor and the spherical components of the operator $\Delta \boldsymbol{N}^{(1)}$ are defined by

$$\Delta N_q^{(1)}=\sum_j \boldsymbol{\beta}_j \boldsymbol{\Sigma}_{qj}, \tag{19}$$

where $\boldsymbol{\Sigma}_{qj}$ is the relativistic spin matrix and $\boldsymbol{\beta}_j$ denotes the Dirac matrices. For a given configuration, Eq. (18) is related to only quantum numbers. The present calculated results are −0.0007733(49) and 0.0007733(42) for the $^2P_{1/2}$ and $^2P_{3/2}$ states, respectively. The present results are in good agreement with the calculations of Verdebout *et al.* [37], Marques *et al.* [38], and Maison *et al.* [36], who used the same corrections as ours. In addition, the present results are still different from the results of Refs. [28,31–35]. The main reason for this discrepancy is that the binding and screening effects [28,31–35] are not included in our calculations.

Nuclear recoil also has an effect on the g factors [31–35,72–76]. The presently calculated contributions of the nuclear recoil which are included in the Hamiltonian are 2.2×10^{-8} and 1.3×10^{-9} for the $^2P_{1/2}$ and $^2P_{3/2}$ states, respectively, as shown in Table XII. These results are several orders smaller than the results of Refs. [31–35,72–74]. Actually, similar to the QED effects, the nuclear recoil contributions are not described completely in the present calculations [31–35,72–76]. So we will do more studies on corrections by nuclear recoil in the future.

TABLE XIII. Calculated g factors of the $2s^2 2p\ ^2P_{1/2}$ and $^2P_{3/2}$ states of Ar^{13+} ions in comparison with those of previous studies. The uncertainties are given in parentheses. The $\Delta g_{\rm QED}$ values of Refs. [28, 31–35] include the contributions of one-loop and two-loop QED.

	$2s^2 2p\ ^2P_{1/2}$		$2s^2 2p\ ^2P_{3/2}$	
Contribution	This work	Other studies	This work	Other studies
g_D	0.663775447	0.663775447 [31]	1.331030389	1.331030389 [31]
$\Delta g_{\rm PS}$	0.0007179		0.0005432	
$\Delta g_{\rm NS}$	−0.0000669		−0.0000608	
$\Delta g_{\rm EEI}(\Delta g_{\rm PS}+\Delta g_{\rm NS})$	0.0006510(9)	0.0006500(8) [31]	0.0004824(26)	0.0004812(30) [31]
		0.0006500(4) [32]		0.0004782(30) [32]
		0.0006506(7) [33]		0.000482(3) [36]
		0.00064996(20) [28]		0.0004787(6) [34]
		0.000651(3) [36]		0.000483 [30]
		0.0006499(4) [35]		
		0.0006518 [30]		
$\Delta g_{\rm QED}$	−0.0007733(49)	−0.0007687(5) [31]	0.0007733(42)	0.0007784(8) [31]
		−0.0007687(5) [32]		0.0007784(8) [32]
		−0.0007681(9) [33]		0.000773(3)(6) [36]
		−0.0007682(2) [28]		0.0007783(12) [34]
		−0.000774(3)(6) [36]		0.00077 [30]
		−0.0007682(2) [35]		
		−0.00078 [30]		
Total	0.6636531(50)	0.663647(1) [31]	1.3322861(49)	1.332285(3) [31]
		0.6636477(7) [32]		1.332282(3) [32]
		0.6636488(12) [33]		1.332286(3)(6) [36]
		0.66364812(58) [28]		1.3322825(14) [34]
		0.663652(3)(6) [36]		1.33228 [30]
		0.6636481(5) [35]		1.332365 [37]
		0.66365 [30]		1.332372(1) [38]
		0.663728 [37]		
		0.663899(2) [38]		
Expt.		0.66364845532(93) [28]		1.3322895(13)(56) [29]
		0.663(7) [30]		1.333(2) [30]

Table XIII lists the g factors of the $^2P_{1/2}$ and $^2P_{3/2}$ states and the contributions of different effects, along with a comparison with some available theoretical results [28–38] as well as the experimental results [28,29]. $\Delta g_{\rm EEI}$ represents the contribution of the total electron-electron interaction, which is the summation of the contributions of the positive-energy states, Breit interaction, and negative-energy states. We find that $\Delta g_{\rm EEI}$ are in good agreement with the results of the large scale configuration interaction approach in the basis of the Dirac-Fock-Sturm orbitals (CI-DFS) [30], the first order within perturbation theory (PT), second- and higher-order CI-DFS [28,31,32,35], first- and second-order PT [33,34], and the RCC [36]. The present total values of 0.6636531(50) and 1.3322861(49) for the $^2P_{1/2}$ and $^2P_{3/2}$ states, respectively, agree with the most accurate experimental results [28,29] very well. The differences are 4.6×10^{-6} and 3.4×10^{-6}.

Through the above comparison, we can find that there are two main reasons for the discrepancy between the existing multiconfiguration Dirac-Fock calculations [37,38] and the experimental results [28,29]. One is that the electronic correlation was not fully considered in both calculations. In Ref. [38], the active space was generated by SD excitations to $n_{\rm max} = 5$, and the single-reference configuration was used. Therefore, there were only 1772 and 2943 CSFs included for $^2P_{1/2}$ and $^2P_{3/2}$, respectively. In Ref. [37], although $n_{\rm max} = 9$ active space was applied and a multi-reference-configuration calculation was performed, the authors included only partial SD excitations from the reference configurations, and their CSF numbers were much lower than the present calculations. The other is that the contributions of negative-energy states were not included in their final results. As a result, the electronic correlation effect in these two calculations is incomplete.

IV. CONCLUSIONS

By using the MCDHF method and RCICP method, the wave functions and energy levels of the low-lying states of the $2s^22p$ and $2s2p^2$ configurations and the single-electron excited states of $2s^2nl$ $(n \geqslant 3; l = s, p, d)$ configurations of Ar^{13+} ions were calculated. The absorption oscillator strengths and transition probabilities were then obtained. A detailed discussion of the contributions of the electron correlation effects, Breit interaction, QED effects, and nuclear recoil to these atomic parameters was also presented. The present results are in good agreement with available theoretical calculations and experimental measurements from the NIST tabulations. The electric dipole polarizabilities of the $2s^22p\ ^2P_{1/2,\ 3/2}$ states, which are dominated by the transitions from the states of $2s2p^2$ and $2s^2nl$ $(n = 3, 4; l = s, d)$, were determined accurately and showed good agreement with the RCC results with a difference of no more than 0.5%. Regarding the g factors of $2s^22p\ ^2P_{1/2,3/2}$ states, the present theoretical values are in agreement to 10^{-6} with the most accurate experiments [28,29].

Although our calculated results are in good agreement with the experimental data, there are still some open problems that need to be solved. For example, in terms of the contributions of QED effects to the g factors, the binding and screening effects [28,31–35,77] are not included in our calculations, and our results are still different from those in the Refs. [28,31–35]. As for the contribution of nuclear recoil to the g factors, only the NMS and SMS are included in the present calculations; the other significant operators [31–35,72–76] are not included yet, and the present calculations underestimate this effect compared with some available results [31–35,72–74]. In terms of radiation transition, the correction of the transition operator by QED effects [78] is not considered. Therefore, we will undertake detailed studies on these issues.

ACKNOWLEDGMENTS

This work has been supported by the National Key Research and Development Program of China under Grant No. 2017YFA0402300; the National Natural Science Foundation of China under Grants No. 12174316, No. 11774292, No. 11804280, No. 11874051, and No. 11864036; the Young Doctor Fund of Gansu Provincial Department of Education under Grant No. 2021QB-017; and the Young Teachers Scientific Research Ability Promotion Plan of Northwest Normal University (Grant No. NWNU-LKQN2020-10).

[1] P. Beiersdorfer, J. Phys. B **48**, 144017 (2015).
[2] J. D. Gillaspy, J. Phys. B **34**, R93 (2001).
[3] C. T. Chantler, M. N. Kinnane, J. D. Gillaspy, L. T. Hudson, A. T. Payne, L. F. Smale, A. Henins, J. M. Pomeroy, J. N. Tan, J. A. Kimpton, E. Takacs, and K. Makonyi, Phys. Rev. Lett. **109**, 153001 (2012).
[4] D. A. Glazov, F. Köhler-Langes, A. V. Volotka, K. Blaum, F. Heiße, G. Plunien, W. Quint, S. Rau, V. M. Shabaev, S. Sturm, and G. Werth, Phys. Rev. Lett. **123**, 173001 (2019).
[5] A. V. Volotka, D. A. Glazov, V. M. Shabaev, I. I. Tupitsyn, and G. Plunien, Phys. Rev. Lett. **112**, 253004 (2014).
[6] V. A. Yerokhin, K. Pachucki, M. Puchalski, Z. Harman, and C. H. Keitel, Phys. Rev. A **95**, 062511 (2017).
[7] V. M. Shabaev, D. A. Glazov, N. S. Oreshkina, A. V. Volotka, G. Plunien, H.-J. Kluge, and W. Quint, Phys. Rev. Lett. **96**, 253002 (2006).
[8] V. A. Yerokhin, E. Berseneva, Z. Harman, I. I. Tupitsyn, and C. H. Keitel, Phys. Rev. Lett. **116**, 100801 (2016).
[9] S. Sturm, F. Köhler, J. Zatorski, A. Wagner, Z. Harman, G. Werth, W. Quint, C. H. Keitel, and K. Blaum, Nature (London) **506**, 467 (2014).
[10] P. J. Mohr, D. B. Newell, and B. N. Taylor, Rev. Mod. Phys. **88**, 035009 (2016).
[11] J. C. Berengut, V. A. Dzuba, and V. V. Flambaum, Phys. Rev. A **84**, 054501 (2011).
[12] J. C. Berengut, V. A. Dzuba, V. V. Flambaum, and A. Ong, Phys. Rev. Lett. **106**, 210802 (2011).
[13] J. C. Berengut, V. A. Dzuba, V. V. Flambaum, and A. Ong, Phys. Rev. A **86**, 022517 (2012).
[14] J. C. Berengut, V. A. Dzuba, V. V. Flambaum, and A. Ong, Phys. Rev. Lett. **109**, 070802 (2012).

[15] A. Derevianko, V. A. Dzuba, and V. V. Flambaum, Phys. Rev. Lett. **109**, 180801 (2012).

[16] V. A. Dzuba, A. Derevianko, and V. V. Flambaum, Phys. Rev. A **86**, 054501 (2012).

[17] V. A. Dzuba, A. Derevianko, and V. V. Flambaum, Phys. Rev. A **86**, 054502 (2012).

[18] V. A. Dzuba, M. S. Safronova, U. I. Safronova, and V. V. Flambaum, Phys. Rev. A **92**, 060502(R) (2015).

[19] Y. M. Yu and B. K. Sahoo, Phys. Rev. A **99**, 022513 (2019).

[20] D. K. Nandy and B. K. Sahoo, Phys. Rev. A **94**, 032504 (2016).

[21] L. Schmöger, O. O. Versolato, M. Schwarz, M. Kohnen, A. Windberger, B. Piest, S. Feuchtenbeiner, J. Pedregosa-Gutierrez, T. Leopold, P. Micke, A. K. Hansen, T. M. Baumann, M. Drewsen, J. Ullrich, P. O. Schmidt, and J. R. C. López-Urrutia, Science **347**, 1233 (2015).

[22] A. Lapierre, U. D. Jentschura, J. R. Crespo López-Urrutia, J. Braun, G. Brenner, H. Bruhns, D. Fischer, A. J. González Martínez, Z. Harman, W. R. Johnson, C. H. Keitel, V. Mironov, C. J. Osborne, G. Sikler, R. Soria Orts, V. Shabaev, H. Tawara, I. I. Tupitsyn, J. Ullrich, and A. Volotka, Phys. Rev. Lett. **95**, 183001 (2005).

[23] A. Lapierre, J. R. Crespo López-Urrutia, J. Braun, G. Brenner, H. Bruhns, D. Fischer, A. J. González Martínez, V. Mironov, C. Osborne, G. Sikler, R. Soria Orts, H. Tawara, J. Ullrich, V. M. Shabaev, I. I. Tupitsyn, and A. Volotka, Phys. Rev. A **73**, 052507 (2006).

[24] I. Draganić, J. R. Crespo López-Urrutia, R. DuBois, S. Fritzsche, V. M. Shabaev, R. S. Orts, I. I. Tupitsyn, Y. Zou, and J. Ullrich, Phys. Rev. Lett. **91**, 183001 (2003).

[25] V. Mäckel, R. Klawitter, G. Brenner, J. R. Crespo López-Urrutia, and J. Ullrich, Phys. Rev. Lett. **107**, 143002 (2011).

[26] V. Mäckel, R. Klawitter, G. Brenner, J. R. Crespo López-Urrutia, and J. Ullrich, Phys. Scr. T **T156**, 014004 (2013).

[27] A. Egl, I. Arapoglou, M. Höcker, K. König, T. Ratajczyk, T. Sailer, B. Tu, A. Weigel, K. Blaum, W. Nörtershäuser, and S. Sturm, Phys. Rev. Lett. **123**, 123001 (2019).

[28] I. Arapoglou, A. Egl, M. Höcker, T. Sailer, B. Tu, A. Weigel, R. Wolf, H. Cakir, V. A. Yerokhin, N. S. Oreshkina, V. A. Agababaev, A. V. Volotka, D. V. Zinenko, D. A. Glazov, Z. Harman, C. H. Keitel, S. Sturm, and K. Blaum, Phys. Rev. Lett. **122**, 253001 (2019).

[29] P. Micke, T. Leopold, S. A. King, E. Benkler, L. J. Spieß, L. Schmöger, M. Schwarz, J. R. Crespo López-Urrutia, and P. O. Schmidt, Nature (London) **578**, 60 (2020).

[30] R. Soria Orts, J. R. Crespo López-Urrutia, H. Bruhns, A. J. González Martínez, Z. Harman, U. D. Jentschura, C. H. Keitel, A. Lapierre, H. Tawara, I. I. Tupitsyn, J. Ullrich, and A. V. Volotka, Phys. Rev. A **76**, 052501 (2007).

[31] D. A. Glazov, A. V. Volotka, A. A. Schepetnov, M. M. Sokolov, V. M. Shabaev, I. I. Tupitsyn, and G. Plunien, Phys. Scr. **T156**, 014014 (2013).

[32] A. A. Shchepetnov, D. A. Glazov, A. V. Volotka, V. M. Shabaev, I. I. Tupitsyn, and G. Plunien, J. Phys.: Conf. Ser. **583**, 012001 (2015).

[33] V. A. Agababaev, D. A. Glazov, A. V. Volotka, D. V. Zinenko, V. M. Shabaev, and G. Plunien, J. Phys.: Conf. Ser. **1138**, 012003 (2018).

[34] V. A. Agababaev, D. A. Glazov, A. V. Volotka, D. V. Zinenko, V. M. Shabaev, and G. Plunien, X-Ray Spectrom. **49**, 143 (2020).

[35] H. Cakir, V. A. Yerokhin, N. S. Oreshkina, B. Sikora, I. I. Tupitsyn, C. H. Keitel, and Z. Harman, Phys. Rev. A **101**, 062513 (2020).

[36] D. E. Maison, L. V. Skripnikov, and D. A. Glazov, Phys. Rev. A **99**, 042506 (2019).

[37] S. Verdebout, C. Nazé, P. Jönsson, P. Rynkun, M. Godefroid, and G. Gaigalas, At. Data Nucl. Data Tables **100**, 1111 (2014).

[38] J. P. Marques, P. Indelicato, F. Parente, J. M. Sampaio, and J. P. Santos, Phys. Rev. A **94**, 042504 (2016).

[39] J. P. Desclaux, Comput. Phys. Commun. **9**, 31 (1975).

[40] P. Jönsson, G. Gaigalas, J. Bieroń, C. F. Fischer, and I. P. Grant, Comput. Phys. Commun. **184**, 2197 (2013).

[41] I. P. Grant, *Relativistic Quantum Theory of Atoms and Molecules: Theory and Computation*, Springer Series on Atomic, Optical, and Plasma Physics (Springer, New York, 2006).

[42] C. F. Fischer, M. Godefroid, T. Brage, P. Jönsson, and G. Gaigalas, J. Phys. B **49**, 182004 (2016).

[43] C. Froese Fischer, G. Gaigalas, P. Jönsson, and J. Bieroń, Comput. Phys. Commun. **237**, 184 (2019).

[44] J. Jiang, J. Mitroy, Y. Cheng, and M. W. J. Bromley, Phys. Rev. A **94**, 062514 (2016).

[45] J. G. Li, P. Jönsson, C. Z. Dong, and G. Gaigalas, J. Phys. B **43**, 035005 (2010).

[46] L. Sturesson, P. Jönsson, and C. Froese Fischer, Comput. Phys. Commun. **177**, 539 (2007).

[47] G. C. Rodrigues, M. A. Ourdane, J. Bieroń, P. Indelicato, and E. Lindroth, Phys. Rev. A **63**, 012510 (2000).

[48] P. J. Mohr, Phys. Rev. Lett. **34**, 1050 (1975).

[49] P. J. Mohr, Phys. Rev. A **26**, 2338 (1982).

[50] P. J. Mohr and Y. K. Kim, Phys. Rev. A **45**, 2727 (1992).

[51] P. J. Mohr, At. Data Nucl. Data Tables **29**, 453 (1983).

[52] S. Klarsfeld and A. Maquet, Phys. Lett. B **43**, 201 (1973).

[53] L. W. Fullerton and G. A. Rinker, Phys. Rev. A **13**, 1283 (1976).

[54] K. G. Dyall, I. P. Grant, C. T. Johnson, F. A. Parpia, and E. P. Plummer, Comput. Phys. Commun. **55**, 425 (1989).

[55] I. P. Grant and H. M. Quiney, Phys. Rev. A **62**, 022508 (2000).

[56] I. P. Grant, *Relativistic Quantum Theory of Atoms and Molecules Theory and Computation* (Springer, New York, 2007).

[57] K. Cheng, Y. K. Kim, and J. P. Desclaux, At. Data Nucl. Data Tables **24**, 111 (1979).

[58] A. N. Artemyev, V. M. Shabaev, I. I. Tupitsyn, G. Plunien, and V. A. Yerokhin, Phys. Rev. Lett. **98**, 173004 (2007).

[59] A. Malyshev, D. Glazov, A. Volotka, I. Tupitsyn, V. Shabaev, and G. Plunien, Nucl. Instrum. Methods Phys. Res., Sect. B **408**, 103 (2017).

[60] A. N. Artemyev, V. M. Shabaev, I. I. Tupitsyn, G. Plunien, A. Surzhykov, and S. Fritzsche, Phys. Rev. A **88**, 032518 (2013).

[61] A. Kramida, Yu. Ralchenko, J. Reader, and NIST ASD Team, NIST Atomic Spectra Database, version 5.9, https://physics.nist.gov/asd.

[62] U. I. Safronova, W. R. Johnson, and M. S. Safronova, At. Data Nucl. Data Tables **69**, 183 (1998).

[63] K. M. Aggarwal, F. P. Keenan, and S. Nakazaki, Astron. Astrophys. **436**, 1141 (2005).

[64] J. Mitroy and M. W. J. Bromley, Phys. Rev. A **68**, 052714 (2003).

[65] P. Rynkun, P. Jönsson, G. Gaigalas, and C. Froese Fischer, At. Data Nucl. Data Tables **98**, 481 (2012).

[66] A. K. Bhatia, U. Feldman, and J. F. Seely, At. Data Nucl. Data Tables **35**, 449 (1986).
[67] S. A. Zapryagaev, Opt. Spectrosc. **47**, 9 (1979).
[68] M. E. Rose, *Elementary Theory of Angular Momentum* (Wiley, New York, 1957).
[69] K. T. Cheng and W. J. Childs, Phys. Rev. A **31**, 2775 (1985).
[70] A. I. Akhiezer, V. B. Berestetskii, and R. A. Shaffer, *Quantum Electrodynamics* (Interscience, New York, 1965).
[71] V. M. Shabaev, D. A. Glazov, M. B. Shabaeva, V. A. Yerokhin, G. Plunien, and G. Soff, Phys. Rev. A **65**, 062104 (2002).
[72] D. A. Glazov and V. M. Shabaev, Phys. Lett. A **297**, 408 (2002).
[73] D. A. Glazov, A. V. Malyshev, V. M. Shabaev, and I. I. Tupitsyn, Opt. Spectrosc. **124**, 457 (2018).
[74] D. A. Glazov, A. V. Malyshev, V. M. Shabaev, and I. I. Tupitsyn, Phys. Rev. A **101**, 012515 (2020).
[75] V. M. Shabaev, Phys. Rev. A **64**, 052104 (2001).
[76] M. Phillips, Phys. Rev. **76**, 1803 (1949).
[77] V. A. Yerokhin and U. D. Jentschura, Phys. Rev. A **81**, 012502 (2010).
[78] V. V. Flambaum and J. S. M. Ginges, Phys. Rev. A **72**, 052115 (2005).